coatings

MDPI

Article

Highly Efficient and Stable $CsPbBr_3$-Alginic Acid Composites for White Light-Emitting Diodes

Muyi Wang [1], Song Wang [1], Renjie Chen [1], Mengmeng Zhu [1], Yunpeng Liu [1], Haojie Ding [1], Jun Ren [1], Tongtong Xuan [2,*] and Huili Li [1,3,*]

[1] Engineering Research Center for Nanophotonics and Advanced Instrument, Ministry of Education, School of Physics and Electronic Science, East China Normal University, Shanghai 200241, China; sent_my@163.com (M.W.); icevcsong@outlook.com (S.W.); 52184700021@stu.ecnu.edu.cn (R.C.); mmzhu910@126.com (M.Z.); 52184700022@stu.ecnu.edu.cn (Y.L.); greatdruidhj@126.com (H.D.); 10195300418@stu.ecnu.edu.cn (J.R.)

[2] Fujian Key Laboratory of Surface and Interface Engineering for High Performance Materials, College of Materials, Xiamen University, Xiamen 361005, China

[3] Chongqing Key Laboratory of Precision Optics, Chongqing Institute of East China Normal University, Chongqing 401120, China

* Correspondence: ttxuan@xmu.edu.cn (T.X.); hlli@phy.ecnu.edu.cn (H.L.)

Abstract: All-inorganic perovskite nanocrystals (NCs) have attractive potential for applications in display and lighting fields due to their special optoelectronic properties. However, they still suffer from poor water and thermal stability. In this work, green $CsPbBr_3$-alginic acid ($CsPbBr_3$-AA) perovskite composites were synthesized by an in situ hot-injection process which showed a high photoluminescence quantum yield (PLQY) of 86.43% and improved moisture and thermal stability. Finally, white light-emitting diodes (WLEDs) were fabricated by combining the green $CsPbBr_3$-AA perovskite composites with red K_2SiF_6:Mn^{4+} phosphors and blue InGaN LED chips. The WLEDs show a relatively high luminous efficacy of 36.4 lm/W and a wide color gamut (124% of the National Television System Committee). These results indicate that the green $CsPbBr_3$-AA perovskite composites have great potential applications in backlight displays.

Keywords: perovskites; in situ hot-injection process; luminescent materials; stability; light-emitting diodes

check for updates

Citation: Wang, M.; Wang, S.; Chen, R.; Zhu, M.; Liu, Y.; Ding, H.; Ren, J.; Xuan, T.; Li, H. Highly Efficient and Stable $CsPbBr_3$-Alginic Acid Composites for White Light-Emitting Diodes. *Coatings* **2023**, *13*, 1062. https://doi.org/10.3390/coatings13061062

Academic Editor: Emerson Coy

Received: 28 April 2023
Revised: 29 May 2023
Accepted: 31 May 2023
Published: 7 June 2023

Copyright: © 2023 by the authors. Licensee MDPI, Basel, Switzerland. This article is an open access article distributed under the terms and conditions of the Creative Commons Attribution (CC BY) license (https://creativecommons.org/licenses/by/4.0/).

1. Introduction

In recent years, we have witnessed a rapid development in the synthesis and application of all-inorganic $CsPbX_3$ (X = Cl, Br and I) perovskite NCs [1–3]. Compared with traditional semiconductor NCs (e.g., CdSe and InP-based NCs), they have better optical properties, such as broadband absorption, tunable emission wavelength, narrow full width at half maximum (FWHM), and high photoluminescence PLQY [4–6], which provides them with potential applications in light emitting diodes (LEDs) [7–9], solar cells [10–12], photodetectors [13–15], photocatalysis [16,17], lasers [18], displays [19], bioimaging [20], and anti-counterfeiting [21].

Although $CsPbX_3$ NCs possess many excellent properties, they are still far from practical applications due to their poor stability [21]. First, the ionic properties of the NCs make them easy to decompose when they are in contact with polar solvents. Second, organic ligands such as oleic acid and oleylamine are widely used in the synthesis of perovskite NCs, which are easily detached from the surface of NCs during the purification process, resulting in a significant decrease in colloidal stability and PLQY. Third, when the colloidal NC solution is solidified into powder (including solidification with encapsulant), the emission of aggregated fluorescence is quenched, and the PLQY decreases sharply.

To address these issues, matrix encapsulation has been carried out to enhance the photoluminescence (PL) stability by embedding perovskite NCs into transparent and stable

matrix materials to form composite luminescent materials [22]. For example, SiO_2 [23], Al_2O_3 [23], KCl, KBr, ZIF-8 [24,25], UiO-67 [26], PMMA [27], and PMAO [27] have been employed as matrices to prepare perovskite composites with enhanced stability. Among them, organic polymers have unique advantages in improving the stability of perovskite NCs. The polymer can form chemical bonds with the surface ions of perovskite due to abundant groups of the polymer, passivating their surface defects and tightly wrapping the NCs to isolate water and oxygen [28–31].

Alginic acid (AA) is a naturally occurring edible polysaccharide [32,33]. It has many carboxyl and hydroxyl groups, and can easily combine with metal ions (such as sodium and calcium) to form the corresponding salt, called alginate. Thus, AA with abundant carboxyl and hydroxyl groups can be used as a surface ligand for perovskite NCs, while its long-chain structure helps to wrap perovskite NCs, forming a matrix structure. In addition, AA is easy to obtain, has abundant material sources and is of extremely low cost, which is also particularly important for late-stage WLEDs applications.

In this study, we successfully synthesized green $CsPbBr_3$-AA perovskite composites using AA as matrix materials and surface ligands by a hot-injection process. The as-prepared perovskite composites not only show excellent optical properties with a high PLQY of 86.43% and a narrow FWHM of 23 nm, but also exhibit high stability against moisture and heat. Furthermore, WLEDs were fabricated by combining green $CsPbBr_3$-AA perovskite composites with red $K_2SiF_6:Mn^{4+}$ phosphors and blue InGaN LED chips. The WLEDs show relatively high efficiency and a wide color gamut.

2. Materials and Methods

2.1. Chemicals

Cesium carbonate (Cs_2CO_3, Alfa Aesar (Shanghai, China), 99%), oleic acid (OA, Damas-beta (Shanghai, China), 90%+), oleylamine (OLA, Damas-beta (Shanghai, China), 90%+), 1-octadecene (ODE, Adamas, 90%), lead (II) bromide ($PbBr_2$, Adamas (Shanghai, China), 99.9%), alginic acid ($(C_6H_8O_6)_n$, Adamas (Shanghai, China), 99%), ethanol (99%), and toluene (C_7H_8, SCRC (Shanghai, China), $\geq$99.5%) were purchased from SINOPHARM and used without further purification.

2.2. Synthesis of Cesium Oleate (Cs-OA) Precursor

A total of 0.420 g of Cs_2CO_3, 1.5 mL of OA, and 20 mL of ODE were added into a 50 mL three-necked flask, which was kept relatively sealed. The mixture was then vigorously stirred and dried under N_2 flow for 1 h at 120 °C. The reaction vessel was swiftly heated to 150 °C and stirred at this temperature for 5 h. After the reaction was completed, the precursor Cs-OA for hot injection were obtained, and were preheated to 100 °C when used.

2.3. Synthesis of $CsPbBr_3$ NCs

$PbBr_2$ (0.1835 g), 1.5 mL of OA, 1.5 mL of OLA, and 15 mL of ODE were added to a 50 mL three-necked flask, which was kept relatively sealed. The mixture was then vigorously stirred and dried under N_2 flow for 1 h at 120 °C. The reaction vessel was swiftly heated to 160 °C for 1 min under N_2 flow, and then Cs-Oleate (1 mL) was swiftly injected into the mixture solution. After 10 s, the reaction solution was cooled to room temperature in an ice water bath. The product solution was centrifuged at 11,000 rpm for 15 min, and the supernatant was subsequently discarded. The precipitated NCs were then redispersed in toluene for further centrifugation at 11,000 rpm for 10 min. The precipitate was dried in a vacuum drying oven at 36.5 °C for 24 h, and the solid samples were stored for characterization.

2.4. Synthesis of $CsPbBr_3$-AA Perovskite Composites

$PbBr_2$ (0.1835 g), x mmol (x = 1, 1.5, 3, 4.5, 6, 7.5) of AA, 1.5 mL of OA, 1.5 mL of OLA, and 15 mL of ODE were added to a 50 mL three-necked flask, which was kept relatively sealed. The mixture was then vigorously stirred and dried under N_2 flow for

1 h at 120 °C. The reaction vessel was swiftly heated to 160 °C for 1 min under N_2 flow, and then Cs-Oleate (1 mL) was swiftly injected into the mixture solution. After 10 s, the solution was cooled to room temperature in an ice water bath. The product solution was centrifuged at 11,000 rpm for 15 min, and the supernatant was subsequently discarded. The precipitate was then redispersed in toluene for further centrifugation at 11,000 rpm for 10 min. The precipitate was dried in a vacuum drying oven at 36.5 °C for 24 h, and the solid samples were stored for characterization.

2.5. Characterization

The XRD pattern was obtained from a Bruker D8 Advance X-ray diffractometer equipped with monochromatic Cu-Kα radiation (λ = 0.154056 nm) as an X-ray source. The X-ray photoelectron spectroscopy (XPS) spectra were acquired by an ESCALAB 250XI system produced by Thermo Scientific. The micromorphology of perovskite NCs was detected by transmission electron microscopy (TEM) and high-resolution transmission electron microscopy (HRTEM), and images were collected by a JEM2100F electron microscope with a 200 kV accelerating voltage. The optical properties were declared through PL and UV/visible absorption spectra using a FluoroMax-4HORIBAs spectrophotometer and a HITACHI U-3900 spectrophotometer, respectively.

3. Results and Discussion

As shown in Figure 1a, X-ray diffraction (XRD) was performed to confirm the successful synthesis of the $CsPbBr_3$-AA composites. Compared with the XRD pattern of pure $CsPbBr_3$ NCs (54-0752), the XRD pattern of $CsPbBr_3$-AA shows characteristic peaks consistent with pure $CsPbBr_3$ NCs. However, since the background peak of AA itself is particularly strong, this characteristic peak is not particularly pronounced, which may be because the wrap of AA is too thick.

From the FTIR spectra of the three samples (Figure 1b), it can be further determined that, compared with the original $CsPbBr_3$ NCs, the intensity of the infrared characteristic peaks corresponding to each organic functional group (C-H, C=O, C-O) in the $CsPbBr_3$-AA composites has been markedly enhanced, which apparently results from the addition of AA. Moreover, we find that after encapsulation, the stretching vibration of -O-H shifts to a low wavenumber by 34 cm^{-1} (3310 cm^{-1} to 3276 cm^{-1}), which indicates that the oxygen atoms are involved in bonding with Pb^{2+}, resulting in an increase in the bond length of the O-H bond and a redshift in the stretching vibration peak. Therefore, a combination of AA and the metal ions on the surface of $CsPbBr_3$ NCs in the $CsPbBr_3$-AA composites can be found.

The XPS energy spectra of $CsPbBr_3$ NCs, AA, and $CsPbBr_3$-AA composites were tested and compared (Figure 1c,d). It is not difficult to find that the oxygen peak (530 eV) and carbon peak (284.8 eV) of the $CsPbBr_3$-AA composites are significantly enhanced compared with those of the original $CsPbBr_3$ NCs, which results from the large amount of organic functional groups from AA. At the same time, it can be seen that the spectra of the $CsPbBr_3$-AA composites show N peaks, Pb peaks, and Br peaks that are consistent with the original $CsPbBr_3$ NCs. These peaks are not available in AA, which indicates the existence of $CsPbBr_3$ NCs in the $CsPbBr_3$-AA composites. However, the Cs peak of the original $CsPbBr_3$ NCs in the spectrum could not be found in the $CsPbBr_3$-AA composites, which may be attributed to the fact that Cs^+ is usually located in the interior of the nanocrystals, and the coating of AA is too thick, so its signal is not obvious. From Figure 1d a new peak appears near 529.5 eV after the high-resolution spectrum of the O 1s orbital is processed by peak separation, which is presumed to be the Pb-O peak. It is further confirmed that the carboxyl and hydroxyl groups in AA are chemically bonded with the metal ions on the surface of the nanocrystals. This phenomenon passivates mezigzag surfacetal ion defects on the surface of nanocrystals, thereby achieving high luminescence performance.

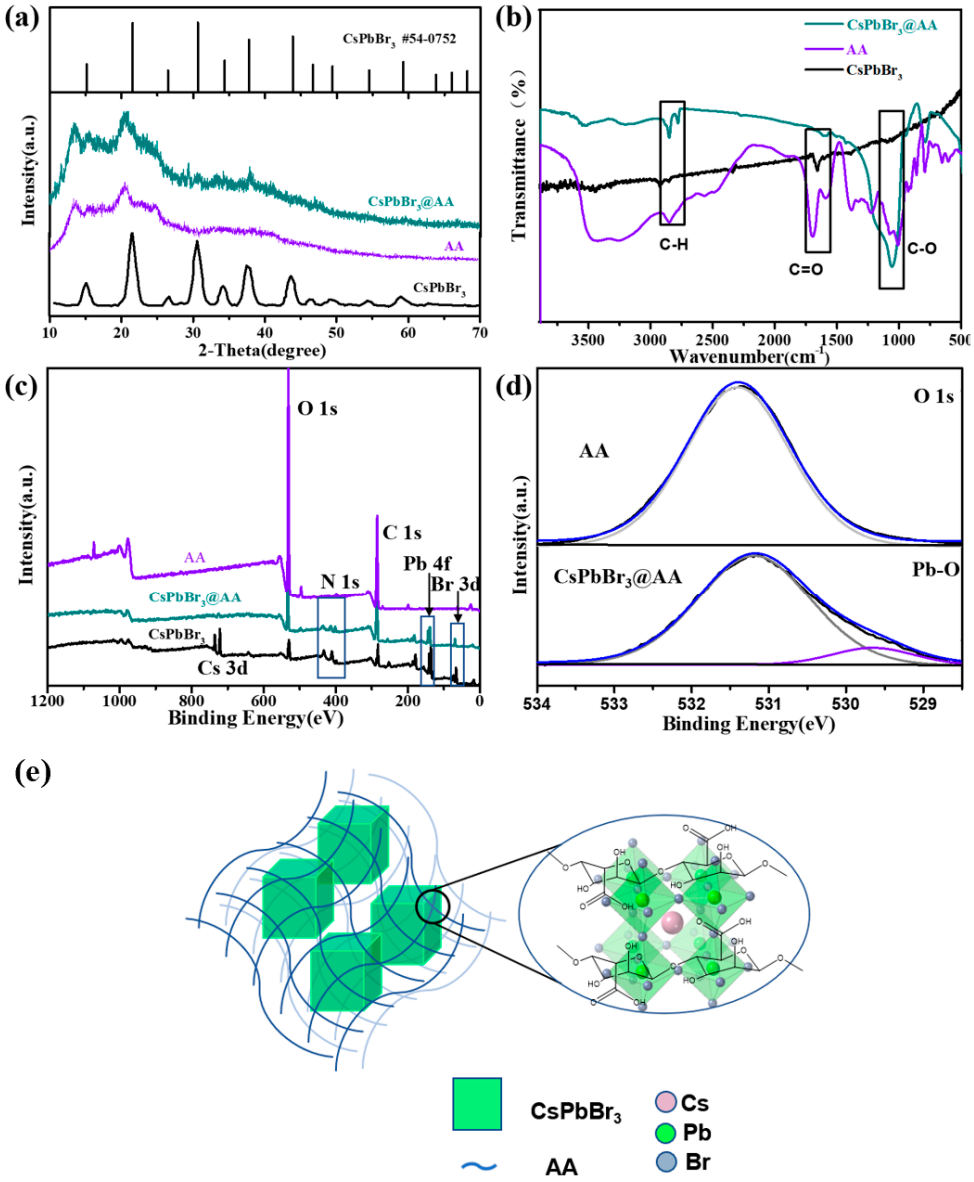

Figure 1. (**a**) XRD patterns of $CsPbBr_3$ NCs and $CsPbBr_3$-AA composites. (**b**) FTIR spectra of AA, $CsPbBr_3$ NCs and the $CsPbBr_3$-AA composite. (**c**) XPS spectra of $CsPbBr_3$ NCs, AA, and $CsPbBr_3$-AA composites. (**d**) High-resolution XPS spectra of O 1 s of AA and $CsPbBr_3$-AA composites. (**e**) Schematic diagram of $CsPbBr_3$-AA composites.

According to the above analysis, we analyzed the encapsulation mechanism of $CsPbBr_3$-AA composites, as shown in Figure 1e. After encapsulation, AA first participates in the formation of nanocrystals through the carboxyl groups contained in it instead of oleic acid, and then a large number of carboxyl groups and hydroxyl groups on the surface of AA are coordinately bonded to the surface of $CsPbBr_3$ NCs, resulting in chemical coordination and the encapsulation of nanocrystals. At the same time, the defects on the nanocrystal surface are passivated, the probability of nonradiative recombination is reduced, and the luminous intensity and quantum efficiency of the composites are significantly improved. At the same time, the flexible long-chain structure of AA can effectively slow the effect of heat on the nanocrystals and enhance their stability.

To further characterize the morphology and structure of the prepared nanocrystals, $CsPbBr_3$ and $CsPbBr_3$-AA were tested by TEM. We can see in Figure 2 that the $CsPbBr_3$ NCs synthesized by the hot-injection process are cubic crystal phases with good dispersibility, and the average particle size is approximately 9.81 nm. After encapsulation with AA,

the $CsPbBr_3$ NCs were embedded in the agglomerated and indistinct organic polymer with stacking, the size distribution of the grains decreased, and the average particle size decreased to 9.57 nm (Figure 2b). The occurrence of this phenomenon may be due to the lack of ligands in the grains, which makes nucleation and growth insufficient and the grains smaller. The further magnification of the local area of the samples, HRTEM, is shown in Figure 2c,d. The measured interplanar spacings of the nanocrystals are 0.29 and 0.41 nm (Figure 2c) and 0.30 and 0.41 nm (Figure 2d), respectively, corresponding to the (200) and (110) planes of the cubic phase $CsPbBr_3$. This shows that in the $CsPbBr_3$-AA composites, the $CsPbBr_3$ NCs are successfully encapsulated by AA. Therefore, the $CsPbBr_3$-AA composite should have significantly improved environmental stability.

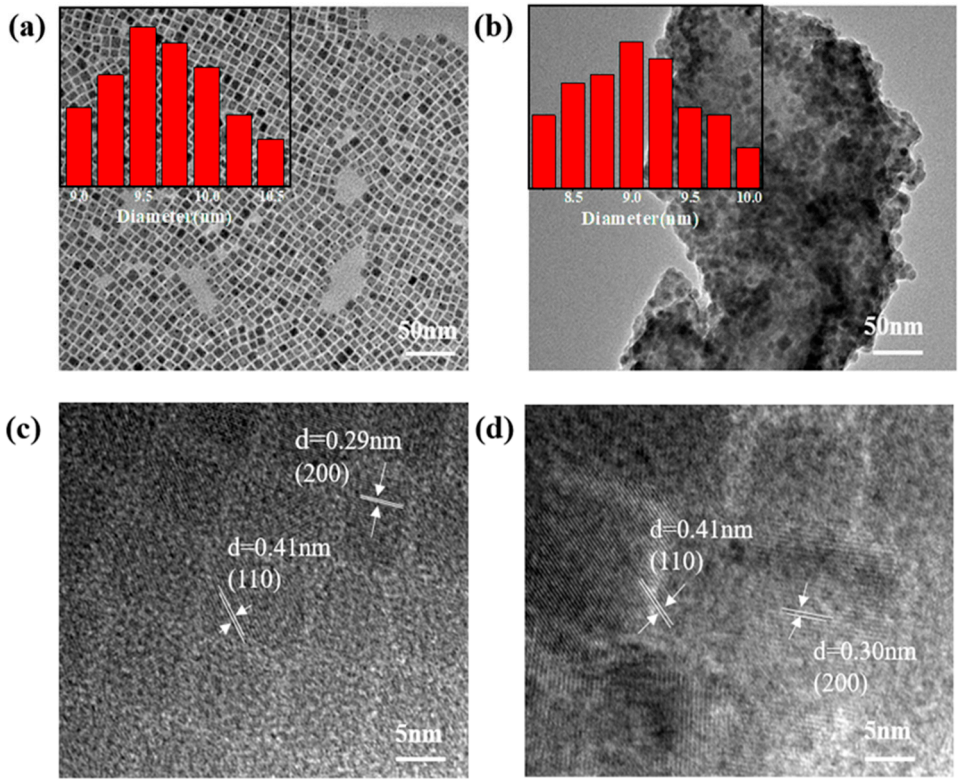

Figure 2. TEM and the corresponding histogram of the particle size distribution (**b**) of the $CsPbBr_3$ NCs (**a**) and $CsPbBr_3$-AA composite (**b**). HRTEM images of the $CsPbBr_3$ NCs (**c**) and $CsPbBr_3$-AA composite (**d**).

We then characterized the fluorescence emission spectra of the samples, as shown in Figure 3a. Compared with the original $CsPbBr_3$ NCs, the fluorescence intensity of the $CsPbBr_3$-AA composites first gradually increased with an increasing AA doping amount and then decreased, which is consistent with the trend shown by the results of the PLQYs test that followed. Moreover, when the doping amount was 3 mmol, the intensity reached the maximum value. Correspondingly, the PLQY increased from 80.93% for the original $CsPbBr_3$ NCs to 86.43% for the $CsPbBr_3$-AA composites. At the same time, a change in the half-peak width was observed. The overall half-peak width of the AA-encapsulated perovskite NCs was wider, and the minimum was 23 nm when the addition amount was 3 mmol, which was still higher than that of the original NCs. It is preliminarily speculated that the encapsulation matrix of AA has a large number of hydroxyl and carboxyl groups. When the concentration is low, the nucleation and growth of NCs is not sufficient due to the absence of oleic acid, resulting in low luminescence performance. When the molar amount of AA increases to a certain extent, this effect is eliminated. At the same time, a large number of carboxyl and hydroxyl groups in the encapsulation matrix can chemically coordinate with the metal ions on the surface of $CsPbBr_3$ NCs, thereby passivating the ionic defects on the surface of the NCs

and finally improving the fluorescence intensity and quantum efficiency of the composites. With a further increase in the amount of AA, too much AA covers the surface of the NCs, and its luminescence performance decreases. In addition, in the fluorescence test, it was found that the emission peaks of the $CsPbBr_3$-AA composites have a redshift compared with the original $CsPbBr_3$ NCs, which is inconsistent with the change in the average particle size. This may be due to the lack of ligands on the surface of NCs with small particle sizes, resulting in increased surface defects and reduced luminescence performance. Although the average particle size is lowered, the luminescent host is still large NCs. As a result, the average particle size decreases while the emission peaks redshift.

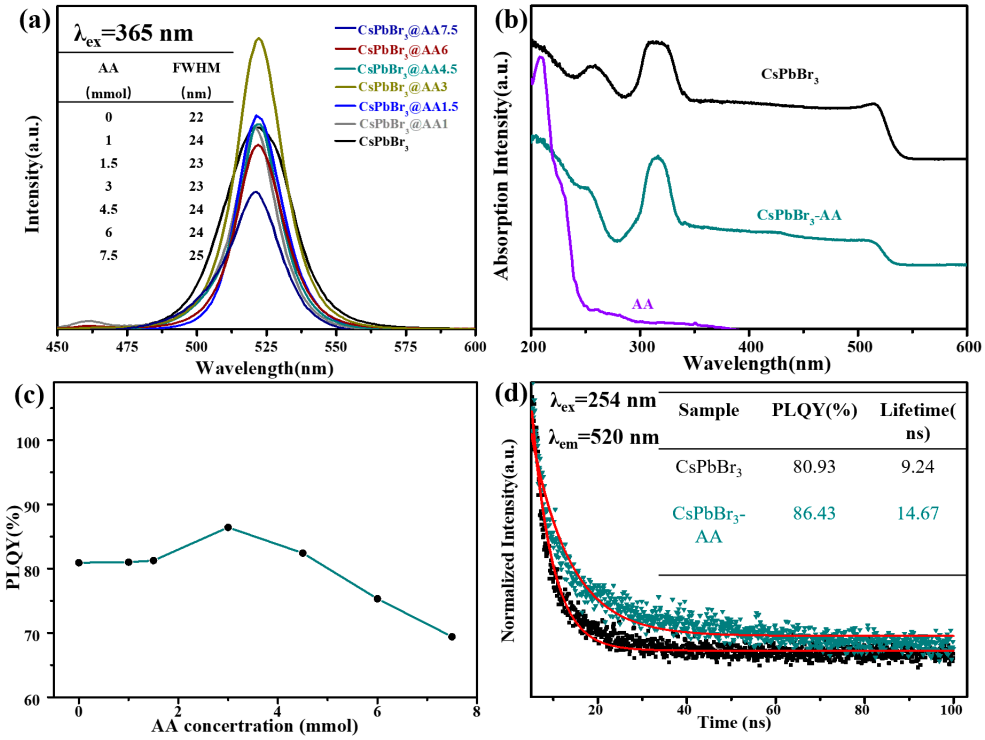

Figure 3. (**a**) PL spectra of pure $CsPbBr_3$ NCs and $CsPbBr_3$-AA composites. (**b**) Absorption spectra of AA, pure $CsPbBr_3$ NCs, and the $CsPbBr_3$-AA composite. (**c**) PLQYs of $CsPbBr_3$ NCs and $CsPbBr_3$-AA composites with different concentrations of AA. (**d**) PL decay curves of $CsPbBr_3$ pure NCs and $CsPbBr_3$-AA composites.

$CsPbBr_3$ NCs, AA and $CsPbBr_3$-AA composites were characterized by UV–Vis absorption spectroscopy and FTIR to reveal the real bonding mode between AA and $CsPbBr_3$ NCs. As shown in Figure 4, compared with the original $CsPbBr_3$ NCs, the absorption spectrum of the $CsPbBr_3$-AA composites is steeper than that of the original $CsPbBr_3$ NCs in the 200–210 nm range, and their position corresponds to the absorption peaks of AA in the same range, which may be due to the addition of AA. At the same time, it was determined that the absorption peaks of the $CsPbBr_3$-AA composites at approximately 510 nm have a redshift compared with the original $CsPbBr_3$ NCs, which is consistent with the emission spectrum.

To verify the above hypothesis, tests for the fluorescence lifetime of $CsPbBr_3$ NCs and $CsPbBr_3$-AA composites were performed. The fluorescence lifetime of perovskite NCs usually exhibits a double exponential decay mode, which can be divided into two parts: a long-lived part (τ_1) and a short-lived (τ_2) part, which correspond to radiative and non-radiative transitions, respectively. The fitted mean life can be based on the following formula [34]:

$$y = A_1 exp\left(-\frac{x}{\tau_1}\right) + A_2 exp\left(-\frac{x}{\tau_2}\right) + y_0 \quad (1)$$

$$\tau_{av} = \frac{\sum A_i \tau_i^2}{\sum A_i \tau_i} \quad (2)$$

Under UV excitation at 254 nm, the fluorescence lifetimes of the original $CsPbBr_3$ NCs and $CsPbBr_3$-AA composites at an emission wavelength of 520 nm were tested and fitted according to Formula (1). The fitting results of τ_1, τ_2 and τ_{av} for all doping concentrations are listed in Table 1. After AA encapsulation, the fluorescence lifetime of the $CsPbBr_3$-AA composites is increased to 14.67 ns. The longer fluorescence lifetime indicates that the defects of the NCs are indeed passivated, and that the nonradiative recombination process of defect-related fast exciton trapping in the pristine $CsPbBr_3$ NCs is effectively eliminated through AA encapsulation. Eventually, the fluorescence intensity and quantum efficiency of the composites increase.

Table 1. PL lifetimes of $CsPbBr_3$ NCs with different contents of AA.

	A_1	τ_1 (ns)	A_2	τ_2 (ns)	τ_{av} (ns)
$CsPbBr_3$	0.64	4.73	0.36	12.27	9.24
$CsPbBr_3$-AA	8.36	0.77	22.51	0.23	14.67

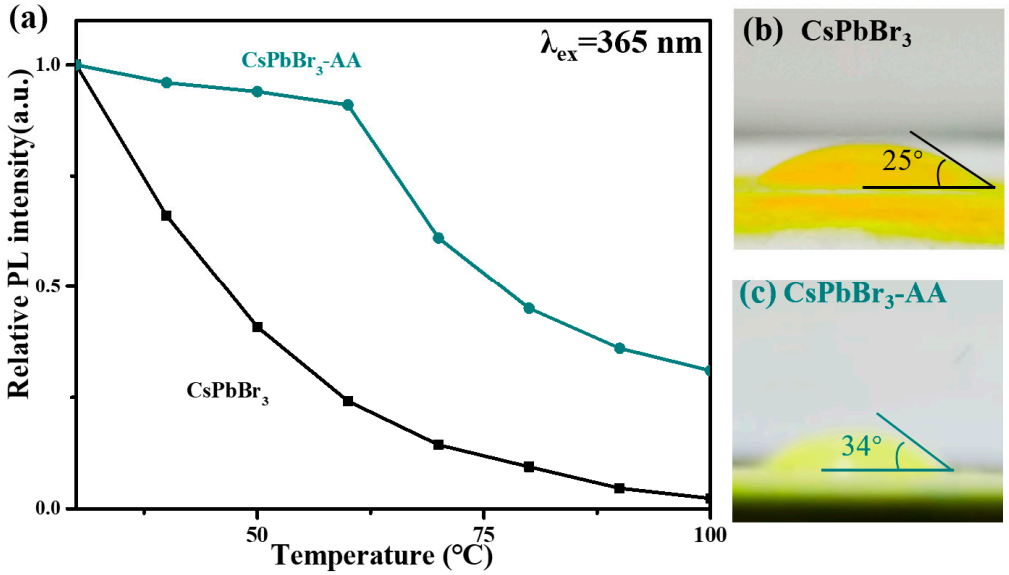

Figure 4. (**a**) Relative PL intensity of the pure $CsPbBr_3$ NCs and $CsPbBr_3$-AA contact angle of $CsPbBr_3$ NCs (**b**) and $CsPbBr_3$-AA (**c**) with water.

To evaluate the thermal stability of the as-prepared composites, we tested the temperature-dependent PL spectra of the $CsPbBr_3$ NCs and the $CsPbBr_3$-AA composites with an excitation wavelength of 365 nm. As shown in Figure 4a, the relative PL intensity of the green $CsPbBr_3$-AA composites maintained 90% of the initial intensity when the environmental temperature was increased to 60 °C, which is higher than that of the pure $CsPbBr_3$ NCs (~15%). Even as the temperature increased to 100 °C, the perovskite composites maintained 30% of the initial value, while the PL of the pure NCs almost disappeared. Furthermore, the contact angle test of water was performed on the $CsPbBr_3$ NC and $CsPbBr_3$-AA composite films. As shown in Figure 4b,c, the $CsPbBr_3$-AA composite films show a contact angle 34° higher than that of the pure $CsPbBr_3$ NC films (25°), which indicates that the composites exhibit better hydrophobicity than the pure NC films. However, the small increase in hydrophobicity is mainly limited by the large number of hydroxyl groups on the surface of AA, and the full consumption of hydroxyl groups cannot be guaranteed during the synthesis process. Due to the excessive hydroxyl groups absorbing water, the hydrophobicity of the composite material is not particularly good.

Finally, we applied the synthesized $CsPbBr_3$-AA composites to white LEDs. A certain amount of $CsPbBr_3$@AA3, K_2SiF_6:Mn^{4+} and AB glue (the mass ratio of a glue to B glue is 1:2) are added into the agate mortar and ground evenly until the bubbles disappear completely. The obtained product was uniformly coated on a gallium nitride (GaN) blue light chip (λ_{em} = 460 nm), which was heated and cured in an oven at 120 °C for 2 h, and the optical properties of the obtained white LED were tested.

As shown in Figure 5, the WLEDs show bright white emission at an operating voltage and current of 3.7 V and 20 mA. The electroluminescence spectrum (EL) contains three characteristic emission peaks, located at 460 nm (blue), 521 nm (green) and 631 nm (red), which belong to the blue LED chips, the green $CsPbBr_3$-AA composites, and red K_2SiF_6:Mn^{4+} phosphor, respectively. The WLEDs exhibit CIE color coordinates of (0.335, 0.344) with a maximum luminous efficiency of 36.4 lm/W. More importantly, the color gamut of the WLEDs can cover over 124% of the NTSC standard, which is much higher than 86% of the traditional phosphor-based WLEDs and 104% of the CdSe-based WLEDs [35–39], which indicates that the green $CsPbBr_3$-AA composites have potential applications in LCD devices.

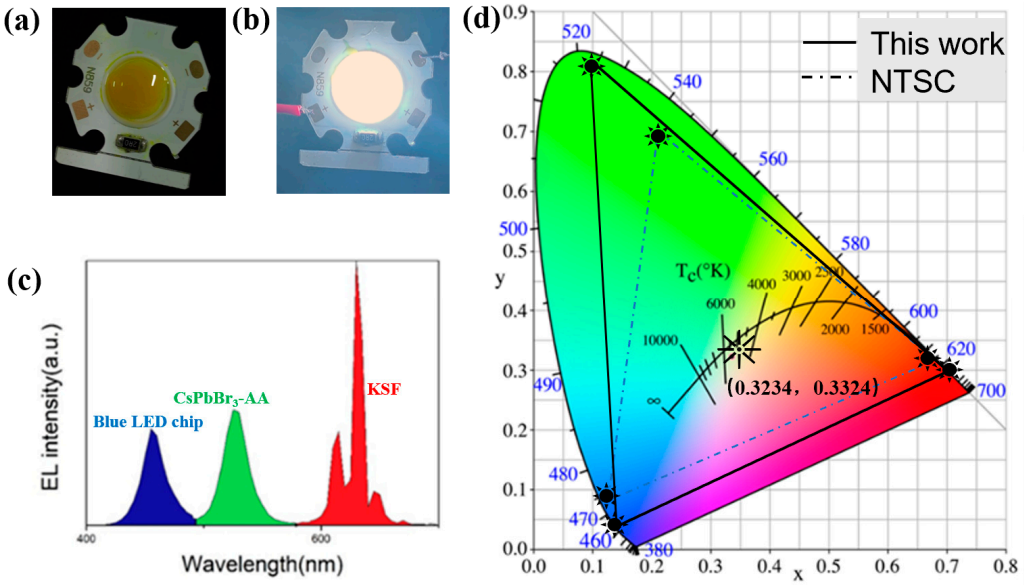

Figure 5. Photographs of (**a**) unlighted and (**b**) lighted of the WLEDs operated at 3.7 V and 20 mA. (**c**) EL spectrum of the WLEDs at 20 mA and 3.7 V, as well as (**d**) the CIE coordinates.

4. Conclusions

In summary, we demonstrated a facile strategy for the synthesis of green $CsPbBr_3$-AA composites using AA as the surface ligand and matrix by a hot-injection method. The green $CsPbBr_3$-AA composites not only preserve a high PLQY of 86.43% and a narrow FWHM of 23 nm, but also show enhanced stability. At 60 °C, the $CsPbBr_3$-AA composites still maintained 90% of the initial intensity, which is much higher than that of the pure $CsPbBr_3$ NCs. Finally, WLEDs were fabricated by combining the green $CsPbBr_3$-AA composites with commercial red K_2SiF_6:Mn^{4+} phosphors and blue LED chips, which exhibited a luminous efficiency of 36.4 lm/W and an ultrawide color gamut of 124% NTSC.

Author Contributions: Conceptualization: M.W., S.W. and T.X.; Methodology: M.W., S.W., R.C., M.Z., Y.L., H.D., J.R., T.X., H.L.; formal analysis: M.W. and S.W.; Investigation: M.W. and S.W.; Resources: All materials, devices and laboratories were provided by the Engineering Research Center for Nanophotonics and Advanced Instrument; Writing—Original Draft: M.W.; Writing—Review & Editing: M.W., T.X. and H.L.; Supervision: T.X. and H.L.; Project Administration: H.L.; Funding Acquisition: T.X. and H.L. All authors have read and agreed to the published version of the manuscript.

Funding: This work was supported by the National Natural Science Foundation of China (No. 12274136), the Chongqing Municipal Natural Science Foundation (No. 33606015, the Chongqing Key Laboratory of Precision Optics, and the Chongqing Institute of East China Normal University, Chongqing 401120, China).

Institutional Review Board Statement: Not applicable.

Informed Consent Statement: Not applicable.

Data Availability Statement: Not applicable.

Acknowledgments: The authors gratefully acknowledge the financial support from the National Natural Science Foundation of China (No. 12274136) and the Chongqing Municipal Natural Science Foundation (No. 33606015, Chongqing Key Laboratory of Precision Optics, Chongqing Institute of East China Normal University, Chongqing 401120, China).

Conflicts of Interest: The authors declare that they have no conflict of interest.

References

1. Cheng, Z.Y.; Lin, J. Layered Organic–Inorganic Hybrid Perovskites: Structure, Optical Properties, Film Preparation, Patterning and Templating Engineering. *CrystEngComm* **2010**, *12*, 2646–2662. [CrossRef]
2. Assirey, E.A.R. Perovskite Synthesis, Properties and Their Related Biochemical and Industrial Application. *Saudi Pharm. J.* **2019**, *27*, 817–829. [CrossRef] [PubMed]
3. Yang, D.; Cao, M.; Zhong, Q.; Li, P.; Zhang, X.; Zhang, Q. All-Inorganic Cesium Lead Halide Perovskite Nanocrystals: Synthesis, Surface Engineering and Applications. *J. Mater. Chem. C* **2019**, *7*, 757–789. [CrossRef]
4. Chen, K.; Jin, W.; Zhang, Y.; Yang, T.; Reiss, P.; Zhong, Q.; Bach, U.; Li, Q.; Wang, Y.; Zhang, H.; et al. High Efficiency Mesoscopic Solar Cells Using $CsPbI_3$ Perovskite Quantum Dots Enabled by Chemical Interface Engineering. *J. Am. Chem. Soc.* **2020**, *142*, 3775–3783. [CrossRef]
5. Protesescu, L.; Yakunin, S.; Bodnarchuk, M.I.; Krieg, F.; Caputo, R.; Hendon, C.H.; Yang, R.X.; Walsh, A.; Kovalenko, M.V. Nanocrystals of Cesium Lead Halide Perovskites ($CsPbX_3$, X = Cl, Br, and I): Novel Optoelectronic Materials Showing Bright Emission with Wide Color Gamut. *Nano Lett.* **2015**, *15*, 3692–3696. [CrossRef] [PubMed]
6. An, R.; Zhang, F.; Zou, X.; Tang, Y.; Liang, M.; Oshchapovskyy, I.; Liu, Y.; Honarfar, A.; Zhong, Y.; Li, C.; et al. Photostability and Photodegradation Processes in Colloidal $CsPbI_3$ Perovskite Quantum Dots. *ACS Appl. Mater. Interfaces* **2018**, *10*, 39222–39227. [CrossRef]
7. Luo, D.; Chen, Q.; Qiu, Y.; Zhang, M.; Liu, B. Device Engineering for All-Inorganic Perovskite Light-Emitting Diodes. *Nanomaterials* **2019**, *9*, 1007. [CrossRef]
8. Du, X.; Wu, G.; Cheng, J.; Dang, H.; Ma, K.; Zhang, Y.-W.; Tan, P.-F.; Chen, S. High-Quality $CsPbBr_3$ Perovskite Nanocrystals for Quantum Dot Light-Emitting Diodes. *RSC Adv.* **2017**, *7*, 10391–10396. [CrossRef]
9. Veldhuis, S.A.; Ng, Y.F.; Ahmad, R.; Bruno, A.; Jamaludin, N.F.; Damodaran, B.; Mathews, N.; Mhaisalkar, S.G. Crown Ethers Enable Room-Temperature Et Ili Synthesis of $CsPbBr_3$ Quantum Dots for Light-Emitting Diodes. *ACS Energy Lett.* **2018**, *3*, 526–531. [CrossRef]
10. Luo, P.; Xia, W.; Zhou, S.; Sun, L.; Cheng, J.; Xu, C.; Lu, Y. Solvent Engineering for Ambient-Air-Processed, Phase-Stable $CsPbI_3$ in Perovskite Solar Cells. *J. Phys. Chem. Lett.* **2016**, *7*, 3603–3608. [CrossRef]
11. Kulbak, M.; Gupta, S.; Kedem, N.; Levine, I.; Bendikov, T.; Hodes, G.; Cahen, D. Cesium Enhances Long-Term Stability of Lead Bromide Perovskite-Based Solar Cells. *J. Phys. Chem. Lett.* **2016**, *7*, 167–172. [CrossRef] [PubMed]
12. Eperon, G.E.; Paterno, G.M.; Sutton, R.J.; Zampetti, A.; Haghighirad, A.A.; Cacialli, F.; Snaith, H.J. Inorganic Caesium Lead Iodide Perovskite Solar Cells. *J. Mater. Chem. A* **2015**, *3*, 19688–19695. [CrossRef]
13. Ramasamy, P.; Lim, D.-H.; Kim, B.; Lee, S.-H.; Lee, M.-S.; Lee, J.-S. All-Inorganic Cesium Lead Halide Perovskite Nanocrystals for Photodetector Applications. *Chem. Comm.* **2016**, *52*, 2067–2070. [CrossRef] [PubMed]
14. Yan, S.; Li, Q.; Zhang, X.; Tang, S.; Lei, W.; Chen, J. A Vertical Structure Photodetector Based on All-Inorganic Perovskite Quantum Dots. *J. Soc. Inf. Disp.* **2020**, *28*, 9–15. [CrossRef]
15. Lv, L.; Xu, Y.; Fang, H.; Luo, W.; Xu, F.; Liu, L.; Wang, B.; Zhang, X.; Yang, D.; Hu, W.; et al. Generalized Colloidal Synthesis of High-Quality, Two-Dimensional Cesium Lead Halide Perovskite Nanosheets and Their Applications in Photodetectors. *Nanoscale* **2016**, *8*, 13589–13596. [CrossRef]
16. Xu, Y.-F.; Yang, M.-Z.; Chen, B.-X.; Wang, X.-D.; Chen, H.-Y.; Kuang, D.-B.; Su, C.-Y. A $CsPbBr_3$ Perovskite Quantum Dot/Graphene Oxide Composite for Photocatalytic CO_2 Reduction. *J. Am. Chem. Soc.* **2017**, *139*, 5660–5663. [CrossRef]
17. Zhang, X.; Qian, Y.; Ling, X.; Wang, Y.; Zhang, Y.; Shi, J.; Shi, Y.; Yuan, J.; Ma, W. Alpha-$CsPbBr_3$ Perovskite Quantum Dots for Application in Semitransparent Photovoltaics. *ACS Appl. Mater. Interfaces* **2020**, *12*, 27307–27315. [CrossRef]
18. Shang, Q.; Li, M.; Zhao, L.; Chen, D.; Zhang, S.; Chen, S.; Gao, P.; Shen, C.; Xing, J.; Xing, G.; et al. Role of the Exciton-Polariton in a Continuous-Wave Optically Pumped $CsPbBr_3$ Perovskite Laser. *Nano Lett.* **2020**, *20*, 6636–6643. [CrossRef]
19. Kovalenko, M.V.; Protesescu, L.; Bodnarchuk, M.I. Properties and Potential Optoelectronic Applications of Lead Halide Perovskite Nanocrystals. *Science* **2017**, *358*, 745–750. [CrossRef]

20. Chen, T.; Huang, M.; Ye, Z.; Hua, J.; Lin, S.; Wei, L.; Xiao, L. Blinking $CsPbBr_3$ Perovskite Nanocrystals for the Nanoscopic Imaging of Electrospun Nanofibers. *Nano Res.* **2021**, *14*, 1397–1404. [CrossRef]
21. Zhu, Z.; Sun, Q.; Zhang, Z.; Dai, J.; Xing, G.; Li, S.; Huang, X.; Huang, W. Metal Halide Perovskites: Stability and Sensing-Ability. *J. Mater. Chem. C* **2018**, *6*, 10121–10137. [CrossRef]
22. Zhang, F.; Shi, Z.-F.; Ma, Z.-Z.; Li, Y.; Li, S.; Wu, D.; Xu, T.-T.; Li, X.-J.; Shan, C.-X.; Du, G.-T. Silica Coating Enhances the Stability of Inorganic Perovskite Nanocrystals for Efficient and Stable Down-Conversion in White Light-Emitting Devices. *Nanoscale* **2018**, *10*, 20131–20139. [CrossRef] [PubMed]
23. Lv, W.; Li, L.; Xu, M.; Hong, J.; Tang, X.; Xu, L.; Wu, Y.; Zhu, R.; Chen, R.; Huang, W. Improving the Stability of Metal Halide Perovskite Quantum Dots by Encapsulation. *Adv. Mater.* **2019**, *31*, 1901–1928. [CrossRef] [PubMed]
24. Bose, R.; Zheng, Y.; Guo, T.; Yin, J.; Hedhili, M.N.; Zhou, X.; Veyan, J.-F.; Gereige, I.; Al-Saggaf, A.; Gartstein, Y.N.; et al. Interface Matters: Enhanced Photoluminescence and Long-Term Stability of Zero-Dimensional Cesium Lead Bromide Nanocrystals via Gas-Phase Aluminum Oxide Encapsulation. *ACS Appl. Mater. Interfaces* **2020**, *12*, 35598–35605. [CrossRef] [PubMed]
25. Zhao, Y.; Xie, C.; Zhang, X.; Yang, P. $CsPbX_3$ Quantum Dots Embedded in Zeolitic Imidazolate Framework-8 Microparticles for Bright White Light-Emitting Devices. *ACS Appl. Nano Mater.* **2021**, *4*, 5478–5485. [CrossRef]
26. Zhang, D.; Zhao, J.; Liu, Q.; Xia, Z. Synthesis and Luminescence Properties of $CsPbX_3$@UIO-67 Composites toward Stable Photoluminescence Convertors. *Inorg. Chem.* **2019**, *58*, 1690–1696. [CrossRef]
27. Zhu, J.; Xie, Z.; Sun, X.; Zhang, S.; Pan, G.; Zhu, Y.; Dong, B.; Bai, X.; Zhang, H.; Song, H. Highly Efficient and Stable Inorganic Perovskite Quantum Dots by Embedding into a Polymer Matrix. *ChemNanoMat* **2019**, *5*, 346–351. [CrossRef]
28. Xin, Y.; Zhao, H.; Zhang, J. Highly Stable and Luminescent Perovskite-Polymer Composites from a Convenient and Universal Strategy. *ACS Appl. Mater. Interfaces* **2018**, *10*, 4971–4980. [CrossRef]
29. Li, Y.; Lv, Y.; Guo, Z.; Dong, L.; Zheng, J.; Chai, C.; Chen, N.; Lu, Y.; Chen, C. One-Step Preparation of Long-Term Stable and Flexible $CsPbBr_3$ Perovskite Quantum Dots/Ethylene Vinyl Acetate Copolymer Composite Films for White Light-Emitting Diodes. *ACS Appl. Mater. Interfaces* **2018**, *10*, 15888–15894. [CrossRef]
30. Wang, Q.; Xu, Y.; Yang, T.; Xue, J.; Wang, Y. Precise Functionalization of a Multiple-Resonance Framework: Constructing Narrowband Organic Electroluminescent Materials with External Quantum Efficiency over 40%. *Adv. Mater.* **2023**, *35*, e2205166. [CrossRef]
31. Tadesse, M.; Dumitrescu, D.; Loghin, C.; Chen, Y.; Wang, L.; Nierstrasz, V. 3D Printing of NinjaFlex Filament onto PEDOT:PSS-Coated Textile Fabrics for Electroluminescence Applications. *J. Electron. Mater.* **2018**, *47*, 2082–2092. [CrossRef]
32. Leid, J.G.; Willson, C.J.; Shirtliff, M.E.; Hassett, D.J.; Parsek, M.R.; Jeffers, A.K. The Exopolysaccharide Alginate Protects Pseudomonas Aeruginosa Biofilm Bacteria from IFN-gamma-mediated Macrophage Killing. *J. Immunol.* **2005**, *175*, 7512–7518. [CrossRef] [PubMed]
33. Lund-Palau, H.; Turnbull, A.R.; Bush, A.; Bardin, E.; Cameron, L.; Soren, O.; Wierre-Gore, N.; Alton, E.; Bundy, J.G.; Connett, G.; et al. Pseudomonas Aeruginosa Infection in Cystic Fibrosis: Pathophysiological Mechanisms and Therapeutic Approaches. *Expert Rev. Respir. Med.* **2016**, *10*, 685–697. [CrossRef] [PubMed]
34. Xuan, T.; Huang, J.; Liu, H.; Lou, S.; Cao, L.; Gan, W.; Liu, R.-S.; Wang, J. Super-Hydrophobic Cesium Lead Halide Perovskite Quantum Dot-Polymer Composites with High Stability and Luminescent Efficiency for Wide Color Gamut White Light-Emitting Diodes. *Chem. Mater.* **2019**, *31*, 1042–1047. [CrossRef]
35. Kalytchuk, S.; Zhovtiuk, O.; Kershaw, S.V.; Zboril, R.; Rogach, A.L. Temperature-Dependent Exciton and Trap-Related Photoluminescence of CdTe Quantum Dots Embedded in a NaCl Matrix: Implication in Thermometry. *Small* **2016**, *12*, 466–476. [CrossRef]
36. Otto, T.; Mueller, M.; Mundra, P.; Lesnyak, V.; Demir, H.V.; Gaponik, N.; Eychmueller, A. Colloidal Nanocrystals Embedded in Macrocrystals: Robustness, Photostability, and Color Purity. *Nano Lett.* **2012**, *12*, 5348–5354. [CrossRef]
37. Kalytchuk, S.; Zhovtiuk, O.; Rogach, A.L. Sodium Chloride Protected CdTe Quantum Dot Based Solid-State Luminophores with High Color Quality and Fluorescence Efficiency. *Appl. Phys. Lett.* **2013**, *103*, 1013–1017. [CrossRef]
38. Mueller, M.; Kaiser, M.; Stachowski, G.M.; Resch-Genger, U.; Gaponik, N.; Eychmueller, A. Photoluminescence Quantum Yield and Matrix-Induced Luminescence Enhancement of Colloidal Quantum Dots Embedded in Ionic Crystals. *Chem. Mater.* **2014**, *26*, 3231–3237. [CrossRef]
39. Yang, H.; Liu, Y.; Hao, J.; Tang, H.; Ding, S.; Wang, Z.; Fang, F.; Wu, D.; Zhang, W.; Liu, H.; et al. Alloyed Green-Emitting CdZnSes/Zns Quantum Dots with Dense Protective Layers for Stable Lighting and Display Applications. *ACS Appl. Mater. Interfaces* **2021**, *13*, 32217–32225. [CrossRef]

Disclaimer/Publisher's Note: The statements, opinions and data contained in all publications are solely those of the individual author(s) and contributor(s) and not of MDPI and/or the editor(s). MDPI and/or the editor(s) disclaim responsibility for any injury to people or property resulting from any ideas, methods, instructions or products referred to in the content.